Arabian Journal of Chemistry (2023) **16**, 104552

King Saud University

**Arabian Journal of Chemistry**

www.ksu.edu.sa
www.sciencedirect.com

ORIGINAL ARTICLE

# Ascorbic acid supported Carboxymethyl cellulose stabilized silver nanoparticles as optical nanoprobe for $Au^{3+}$ detection in environmental sample

**Titilope John Jayeoye [a,*], Chamaiporn Supachettapun [b], Nongnuj Muangsin [a,c,*]**

[a] *Department of Chemistry, Faculty of Science, Chulalongkorn University, Bangkok 10330, Thailand*
[b] *Program in Petrochemistry and Polymer Science, Faculty of Science, Chulalongkorn University, Bangkok, 10330, Thailand*
[c] *Nanotec-CU Center of Excellence on Food and Agriculture, Department of Chemistry, Faculty of Science, Chulalongkorn University, Bangkok 10330, Thailand*

Received 26 August 2022; accepted 4 January 2023
Available online 13 January 2023

**KEYWORDS**

Carboxymethyl cellulose;
Silver nanoparticles;
Gold (III) ion;
Ascorbic acid;
Colorimetry;
Catalyst

**Abstract** Heavy metals (HMs), pollution of major environmental matrices and its attendant effects on human health and the environment, continue to generate huge scientific interest, particularly in monitoring and detection. Herein, the optical property of carboxymethyl cellulose stabilized silver nanoparticles (CMC-AgNPs), supported with ascorbic acid, is exploited as a colorimetric probe for the detection of toxic $Au^{3+}$ ion in solution. The as-synthesized CMC-AgNPs showed sharp absorption maximum at 403 nm, with sparkling yellow color and average particles size distribution less than 10 nm. It was further characterized using ATR-FTIR, TEM, FESEM/EDS, XRD and DLS/zeta potential analyzer. $Au^{3+}$ ion detection strategy involves the addition of ascorbic acid (AA) to a pH adjusted CMC-AgNPs, followed by the analyte addition. AA would facilitate the reduction of $Au^{3+}$ on CMC-AgNPs (seed), with resultant color perturbations from light yellow to yellow, orange, ruby red and purple red, under 8 min incubation, at room temperature (RT). The CMC-AgNPs could also serve as a catalyst, by promoting AA mediated reduction of $Au^{3+}$, *in-situ*. Moreover, we propose, that the color and the absorption spectra change is attributed to the deposition of gold nanoparticles (AuNPs), on the CMC-AgNPs/AA probe, to form (CMC-Ag@Au) nanostructures, depending on the analyte concentration. Absorbance ratio ($A_{540}/A_{403}$) showed good linearity with $Au^{3+}$ concentration from 0.25 to 100.0 μM, and an estimated LOD of 0.061 μM. The assay was applied to $Au^{3+}$ detection in environmental wastewater sample, showing satisfactory real sample detection potentiality.



* Corresponding authors at: Department of Chemistry, Faculty of Science, Chulalongkorn University, Bangkok 10330, Thailand.
E-mail addresses: titilope12@gmail.com, jayeoye.t@chula.ac.th (T.J. Jayeoye), nongnuj.ms@gmail.com, nongnuj.j@chula.ac.th (N. Muangsin).
Peer review under responsibility of King Saud University.

Production and hosting by Elsevier

https://doi.org/10.1016/j.arabjc.2023.104552

## 1. Introduction

Among the various heavy metals (gold, mercury, lead, cobalt, silver, cadmium, chromium, magnesium, iron etc), considerable attentions are devoted to gold owing to huge applications of gold in jewelry manufacture, as components of electronics and electrical appliances, and in numerous industrial applications such as, medical, automotive, defense and aerospace fields (Corti et al., 2002). From the perspective of toxicity, gold metal is not very toxic. However, gold in ionic forms ($Au^{3+}$), is very toxic. For example, $Au^{3+}$ owing to its high thiophilicity, can bind very strongly to DNA, proteins, amino-acids and enzymes forming complexes/cleaving, and thus impart negatively on the optimal biological performance of such biomolecules (Kambam et al., 2015). Moreover, soluble gold salts, such as gold chloride have been investigated to cause severe damages on organs (spleen, liver, lungs, kidney) (Block and Knapp, 1945). It is also important to state that with the popular applications of gold nanoparticles-fabricated from ($Au^{3+}$) salts, in diverse research areas, the possibility of ($Au^{3+}$) leaching and consequent pollution of various environmental matrices have risen in the past few decades. Consequently, the need for consistent monitoring of ($Au^{3+}$) pollution has attracted increased interest from scientists. Reported detection strategy for ($Au^{3+}$) include; inductively coupled plasma-mass spectrometry ICP-MS (Losev et al., 2020), atomic absorption spectroscopy AAS (Afzali et al., 2014), methods based on electrochemistry (anodic stripping voltammetry) (Hall and Vaive, 1992; Wu and Lai, 2016), fluorescence-based methods (Hazarika et al., 2020; Qin et al., 2021) and methods based on exploiting the optical properties of metal nanoparticles (Megarajan et al., 2019; Tantubay et al., 2021; Yang et al., 2018). These methods can effectively detect ($Au^{3+}$), however, the assays design in terms complex sample preparation steps for AAS and ICP-MS, and the use of some toxic reagents for fluorescence assays, calls for a more robust, sensitive, selective, timely and facile approach for ($Au^{3+}$) detection.

The roles of nanomaterials in plenitude of human scientific engagements have continued to gain wide acceptability owing to their unique physico-chemical properties. In fact, their high surface area to volume ratio, provide a versatile, reliable, and efficacious platform for the incorporation of diverse materials for onward delivery to specific sites. Silver nanoparticles (AgNPs) are notable nanomaterial with huge biomedical interest in view of their high antimicrobial potentiality (Eze et al., 2022; Jayeoye et al., 2021; Jayeoye et al., 2020). Further, AgNPs surface plasmon resonance (SPR) property, which arises from the activation of surface electrons on metals resulting from electromagnetic interaction(Zeng et al., 2017), have been well exploited for the detection of wide-ranging toxic metal ions in solution (Huang et al., 2016; Ismail et al., 2018; Prema et al., 2022; Rajar et al., 2021). In the detection strategies mentioned above, the perturbations in the absorption maximum of AgNPs and its optical properties are well correlated with the concentrations of the various analytes of interest. For example, Duan et al. proposed a colorimetric probe for toxic $Hg^{2+}$ detection, based on the anti-aggregation of citrate stabilized AgNPs (Duan et al., 2014). 6-thioguanine was used to induce the aggregation of AgNPs, in the absence of $Hg^{2+}$. However, with prior mixing of $Hg^{2+}$ and 6-thioguanine, the aggregation effect of 6-thioguanine is prevented, owing to the high binding interaction between them. Consequently, reverse color perturbations was realized, with impressive sensitivity. Moreover, the detection of highly hazardous glyphosate herbicide using AgNPs, supported with laser ablation device was reported (De Góes et al., 2017). The stability of AgNPs is an important property of interest to serve as optical probe. Thus, the changes in the nanoparticles color and absorption spectra can be appropriately related to the concentration of analytes.

Another important feature of metal nanoparticles is their catalytic properties. This property is significant in facilitating the occurrence of some naturally non-feasible reactions. Thus, AgNPs have been employed towards the degradation of numerous contaminants and recalcitrant pharmaceuticals in water (Baghbani-Arani et al., 2017; Mosaviniya et al., 2019; Xu et al., 2020). AgNPs are used to reduce the inherent energy barriers and thus provide a more suitable route towards the successful actualization of the reaction path.

Biopolymers mediated synthesis of metal nanoparticles (MNPs) have opened an exciting vista, especially in tuning the surface corona of nanoparticles. They have been found to modulate the properties of the fabricated MNPs, while also conferring better stability on the material. Their perfect aqueous dispersity, good water solubility, huge availability, affordability, biocompatibility, non-toxicity etc. made biopolymers an important bio-resource with far-reaching applications in the food industry, bio-medical field and pharmacy (Chen et al., 2020). Among the available biopolymers, carboxymethyl cellulose (CMC), is one of the most applied, owing to its good solution forming property in water, biodegradability, non-toxic and edible nature. It is a derivative of cellulose and thus one of the most readily available biopolymers around. It is used in film forming for food packaging and as a perfect reductant of metal salts or as a stabilizing agent in colloidal nanofabrication, arising from its numerous hydroxyl groups (Lin et al., 2022; Madla-Cruz et al., 2020). CMC matrix also provides an environment for the immobilization of metal ions and thus prevents easy leaching of toxic metal ions in solution, which consequently improves the biological properties of MNPs with CMC based synthesis. The stability property of nanomaterials mediated by CMC biopolymer is of huge interest in nanoparticles detection of wide-ranging analytes. The adsorption property of polyvinyl alcohol (PVA)/CMC hydrogel towards metal ions ($Ni^{2+}$, $Zn^{2+}$, $Cu^{2+}$ and $Ag^{+}$) was investigated by (Wang and Wang, 2016). It was revealed that the addition of CMC to PVA to form polymer blend (PVA-CMC) hydrogel, improved the metal ion adsorption property of the hydrogel, especially towards $Ag^{+}$. Encouraged by this, in this work, we used CMC for AgNPs synthesis, owing to its good aqueous dispersity, stability, availability, cost effectiveness and metal ions sensitivities. In fact, it is one of the cheapest biopolymers around, and thus would reduce overall cost of the fabricated CMC-AgNPs.

In this contribution, we exploited the good stabilizing property of CMC to fabricate CMC-AgNPs using highly reductive $NaBH_4$ at room temperature. We used $NaBH_4$ to achieve nanoparticles with low particles sizes inside CMC-matrix, which can improve its catalytic property while serving as seed for the growth of gold nanoparticles, formed via ascorbic reduction of $Au^{3+}$. With the addition of $Au^{3+}$ (analyte), to the CMC-AgNPs, coupled with an external reductant (Ascorbic acid AA), $Au^{3+}$ would be reduced on the CMC-AgNPs seed to form CMC-Ag@Au nanostructure, depending on the concentration of the analyte. With this approach, a fast, sensitive, and selective colorimetric detection strategy was built for $Au^{3+}$ detection in aqueous environment. The detection strategy proposed relied on the use of CMC-AgNPs as a seed/catalyst, under AA support, as detection strategy for $Au^{3+}$. With analyte addition, CMC-Ag@Au nanostructure is formed with distinct optical and absorption spectra property. This assay is different from other reported works where AgNPs is used as detection probe for $Au^{3+}$ through basic redox reaction. To the best of our search, this is the first report of $Au^{3+}$ detection based on this method.

## 2. Experimental section

### 2.1. Reagents

Carboxymethyl cellulose (CMC), degree of substitution 1.2 and molecular weight of 120 kDa, Ascorbic acid (AA) and gold (III) chloride trihydrate ($HAuCl_4{\cdot}3H_2O$) were purchased from Sigma Aldrich. $AgNO_3$ was from RCI Labscan, Thailand. $NaBH_4$ was from LOBA CHEMIE India. Different metal salts used in the selectivity studies include: $Ca(NO_3)_2{\cdot}4H_2O$, $FeCl_3$, $Cr(NO_3)_3$, $HgCl_2$ from LOBA CHEMIE, $MgCl_2{\cdot}6H_2O$ and $MnCl_2{\cdot}4H_2O$ from QReC, $KNO_3$ and $NaNO_3$ from Spectrum Chem Corp USA, $BaCl_2$, $NiCl_2{\cdot}8H_2O$, $CuSO_4{\cdot}5H_2O$, $Al(NO_3)_2{\cdot}9H_2O$ and $ZnSO_4{\cdot}7H_2O$ are all from APS Ajax Finechem ltd., $Pb(NO_3)_2$

and $CdCl_2 \cdot 2..5H_2O$ from Sigma Aldrich, $CoCl_2 \cdot 6H_2O$, $Fe_2SO_4 \cdot 7H_2O$ from Merck. The salts were used without any further purification by dissolving appropriate mass in ultra-pure water, obtained from a Millipore water purification set up.

### 2.2. Instruments

All absorption spectra were acquired on an Agilent 8453 UV–vis spectrophotometer. The images of the CMC-AgNPs and those after $Au^{3+}$ injection, were observed using a transmission electron microscope (TEM) JOEL, JEM 2010 machine while the Field emission scanning electron microscope (FESEM) images (Apreo, FEI) was used to observe the morphology of CMC and CMC-AgNPs film. The FESEM equipment was connected to an energy dispersive X-ray spectroscopy (EDX) set-up (X Max 80, Oxford Instrument, UK). X-ray diffractogram (XRD), was profiled using a XRD diffractometer form Empyrean, with the following features: operating degree (5 to 80°) on a Cu Kα incident beam, having a wavelength of 0.154 nm and a scan speed of 70.2 s. Zeta potential and the hydrodynamic diameter (Dh) were collected on Dynamic Light Scattering (DLS) machine, Malvern ZETASIZER NANO. Appropriately diluted sample was measured into a 1 mL sized capillary cell and then inserted into the sample holder of the equipment. Each sample was run in triplicate and the equipment set for (n = 100) for each run. Nicolet FTIR/ATR iS50 from Thermo-Fisher was used for functional group elucidation, by taking wavelength between 4000 and 500 $cm^{-1}$. Raman spectra were obtained using Raman microscope spectrometer, RAMANforce from Nanophoton. All photo images were acquired on a Samsung A50 Android phone.

### 2.3. Preparation of CMC-AgNPs

0.3 % (w/v) of CMC was prepared by dissolving appropriate weight in a beaker containing distilled water, under stirring. The mixture was further raised to 60 °C for 2 hrs to form a colorless viscous solution. The CMC solution was stored at RT overnight before use. CMC-AgNPs was synthesized based on reported work (de Lima et al., 2014), with modification. Into an aluminum foil wrapped beaker, 60 mL of 0.15 % CMC solution was measured, then 3 mL of 10 mM of $AgNO_3$ was injected under stirring at RT, 3 mL of chilled, freshly prepared 20 mM $NaBH_4$ was added under vigorous stirring. The solution was further stirred for I hr and then transferred into an amber bottle and stored at 4 °C before use.

### 2.4. Colorimetric detection of $Au^{3+}$

Colorimetric detection of $Au^{3+}$ using CMC-AgNPs was conducted as follows. Into a 5 mL tube, 300 µL of CMC-AgNPs was added, 1300 µL of ultra-pure water was added for dilution, followed by 150 µL of 50 mM NaOH, then 200 µL of 50 mM AA (optimal concentration) and finally, 50 µL of fresh $Au^{3+}$ (with different concentrations) was injected, so that the final concentrations of $Au^{3+}$ ranged from 0.00 to 150.0 µM, in 2 mL reaction volume. The mixture was vortex mixed, incubated at RT for 8 min, after which the photo images and the UV–vis absorption spectra were collected on an Agilent 8450 UV–vis spectrophotometer and Samsung A50 phone respectively.

### 2.5. Real sample preparation

The practical application of CMC-AgNPs/AA sensor for $Au^{3+}$ detection in real sample, was demonstrated, using environmental water sample from the Chulalongkorn University. The water sample was collected in a polypropylene bottle and then refrigerated at 4 °C before use. The refrigerated water sample was removed and allowed to cool to RT. It was filtered using a 0.22-µm syringe filter, to trap out all dissolved solids. Some part of the processed water sample was submitted for ICP-MS to check if there is gold contamination. Then the other part was assessed using our CMC-AgNPs/AA colorimetric probe, by spiking appropriate concentrations of $Au^{3+}$. The accuracy of the probe was expressed as percent recovery, using the equation,

Recovery = $(C_1 - C_0)/C_{std} \times 100$ % where, $C_1$ = concentration of spiked, $C_0$ = concentration of unspiked sample and $C_{std}$ is the concentration of added standard.

## 3. Results and discussion

### 3.1. Synthesis of CMC-AgNPs

In this work, we selected CMC as a stabilizer and $NaBH_4$ as the reductant to obtain a very stable CMC-AgNPs with very small particle sizes, since $NaBH_4$ is a very strong chemical reductant of metal salts. The choice of AgNPs with very small sizes, realized through $NaBH_4$ adoption for synthesis is based on the direct correlation between catalytic proficiency of nanoparticles and their sizes, as reported (Zhou et al., 2010). The addition of aqueous $NaBH_4$ to a mixture of CMC and $AgNO_3$ at RT under stirring, generated a sparkling yellowish CMC-AgNPs. The concentrations of $Ag^+$ in the synthesis pot may have a strong effect on the resulting colloidal nanoparticles and was thus optimized. Adding 3 mL of 1.0, 5.0,10.0, 15.0 and 20.0 mM of $AgNO_3$ solution to fixed 60 mL, 0.15 % CMC and 3 mL 20 mM $NaBH_4$, the final concentrations of $Ag^+$ in the synthesis pot are 0.045, 0.227, 0.455, 0.982 and 0.910 mM respectively. As shown in Fig. 1, the absorption intensity increases as the concentrations of $AgNO_3$, with sparkling yellowish color, except for the first pot (Fig. 1 (a) inset). There existed a sharp absorption maximum at 403 nm, which is attributed to the surface plasmon resonance band of AgNPs with small particle sizes. Further information on the stability of the colloidal solutions (containing different $AgNO_3$ concentrations), could be obtained by plotting the absorbance at 403 and 550 nm. As depicted in Fig. 1(B), the ratio $A_{403}/A_{550}$ increases as $AgNO_3$ concentration and then diminishes after 0.455 mM. This shows synthesis with 0.455 mM $AgNO_3$ furnished CMC-AgNPs with the best colloidal stability, optical property and was thus selected.

### 3.2. Characterization of CMC-AgNPs

CMC and CMC-AgNPs were subjected to different instrumental characterizations to obtain information on the microstructural property of the synthesized materials. The TEM images of CMC-AgNPs, as revealed in Fig. S1, shows spherical and well dispersed images (Fig. S1(A)), while the hydrodynamic diameter from the dynamic light scattering machine (DLS),

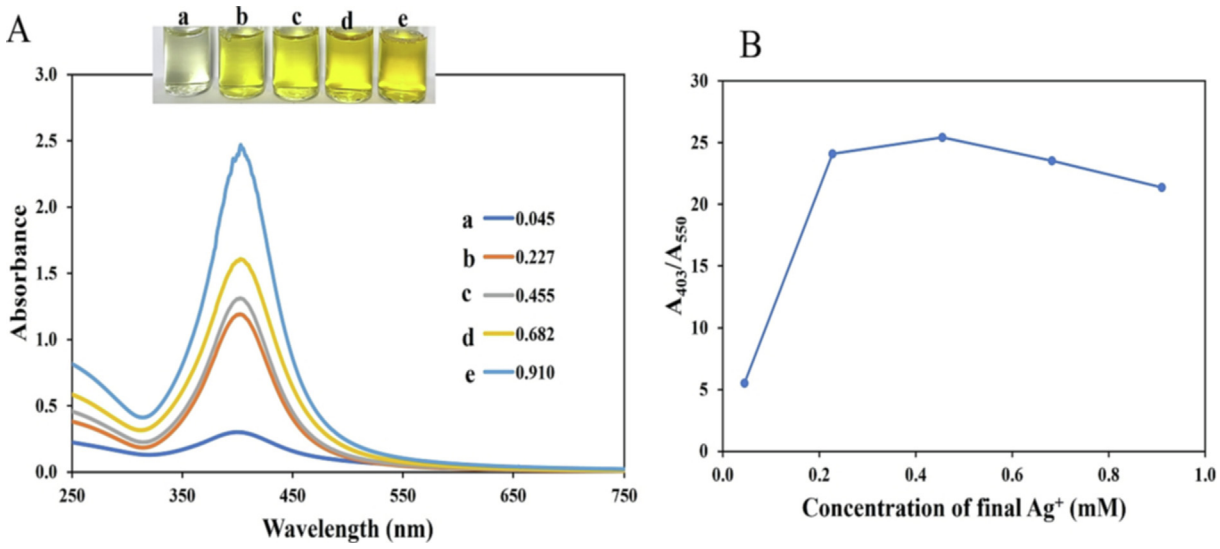


**Fig. 1** (A) UV–vis absorption spectra of CMC-AgNPs, synthesized by varying $AgNO_3$ final concentrations at a. 0.045b. 0.227c. 0.455 d. 0.682 e. 0.910 mM, inset shows the photo images (B) Plot of $A_{403}/A_{550}$ versus the final concentrations of $AgNO_3$.

(Fig. S1(B)), showed particle sizes of 69.8 ± 2.4 nm, with zeta potential value of −17.5 ± 0.5 mV (Fig. S1(C)), attesting to the high stability of the synthesized CMC-AgNPs.

Furthermore, the interaction between biopolymer and nanoparticles was further elucidated using ATR-FTIR. Fig. 2A shows the identified peaks in CMC as: 3300, 2882, 1582, 1410, 1320 and 1010 $cm^{-1}$. These peaks are assigned to the O—H stretching, C—H stretching, C═O asymmetric stretching vibration, $CH_2$ scissoring, C—O bending vibrational peak and the C—H in-plane bending vibrational peak (Asnag et al., 2019). These peaks are all present in the CMC-AgNPs, but are further shifted, which is attributed to the interaction between CMC and the nanoparticles. Fig. 2B, shows the diffraction peaks of CMC and CMC-AgNPs. As contained, sharp peak at 21.3° is conspicuously displayed in CMC, confirming the amorphous nature of CMC biopolymer (Asnag et al., 2019). In the CMC-AgNPs (Fig. 2B), sharp peaks at 20.0, 38.6, 46.3, 64.8, 77.8° are all present. These peaks are assigned to amorphous CMC and (111), (200), (220) and (311) face-centred cubic *(fcc)* crystalline plane of AgNPs. This shows the CMC-AgNPs is reflective of the constituting materials-CMC and the in-situ generated AgNPs. To show, the impact of AgNPs impregnation in CMC matrix, FESEM images of CMC film before and after nanoparticles synthesis were acquired. Fig. 2(C), shows the polymer morphology were smooth without no observable patches, while after AgNPs deposition in the CMC-matrix using $NaBH_4$ based chemical synthesis, white patches of AgNPs could be clearly observed immobilized in CMC polymer matrix (Fig. 2(D)). Moreover, the particles are spherical and dispersed, in consonance with the TEM images above.

The EDS spectra of CMC-AgNPs is displayed in Fig.S2. The identified elemental composition includes C, O, Na, and Ag, which validated the attachment of AgNPs in CMC matrix.

Raman analysis is another reliable analytical tool for probing biopolymers' interaction. As shown in Fig. S3, sharp peak at 1106.4 $cm^{-1}$ is observed in CMC, which is attributed to the C═O stretching vibration (Devi et al., 2020). This peak increased to 1181.4 $cm^{-1}$, in CMC-AgNPs, with the introduction of other notable peaks, arising from the interaction of CMC with AgNPs, in support of the result from ATR-FTIR.

### *3.3. Colorimetric detection of $Au^{3+}$ using CMC-AgNPs*

Metal nanoparticles (MNPs) attraction by scientists in analytical detection continue to gain tremendous acceptability due to their high extinction coefficients, far exceeding those of commonly available fluorophores. Consequently, they have higher absorbing properties (Paramelle et al., 2014). The detection of $Au^{3+}$, proposed in this work was conceptualized by linking the formation of red/purple of AuNPs, in the presence of reducing agent, with $Au^{3+}$ detection. Since the highlighted color above is characteristic of AuNPs only, thus the proposed method is expected to benefit from high selectivity, since only gold nanoparticles is known to shows purple/red color with absorption spectra around 520–550 nm (Krajczewski et al., 2017). Thus, in this assay we adopted AA-an efficient biological reducing agent as the complementary external reducing agent, with CMC-AgNPs as the seed. As metal nanoparticles generally exhibit good catalytic properties (Santos et al., 2012), we believe the CMC-AgNPs will serve as catalyst to promote the reduction of AA in the reaction pot after the analyte ($Au^{3+}$) addition. Fig. 3 shows the interaction between CMC-AgNPs, NaOH, AA on the analyte detection. The absorption spectra of CMC-AgNPs with sharp peak at 403 nm is displayed (Fig. 3(a)), with light yellowish color (Fig. 3(a) inset. The addition of NaOH to CMC-AgNPs for pH adjustment did not induce any significant change in the absorption spectrum (Fig. 3(b)), but a slight color change (Fig. 3(b) inset). The addition of $Au^{3+}$ to CMC-AgNPs and NaOH led to an immediate color fading to colorless. This is due to the redox reaction between $Au^{3+}$ and $Ag^0$. The standard reduction potential of $Au^{3+}/Au^0$ is 0.99 V, while that of $Ag^+/Ag^0$ is 0.80 V. Accordingly, $Au^{3+}$ can induce the oxidation of AgNPs

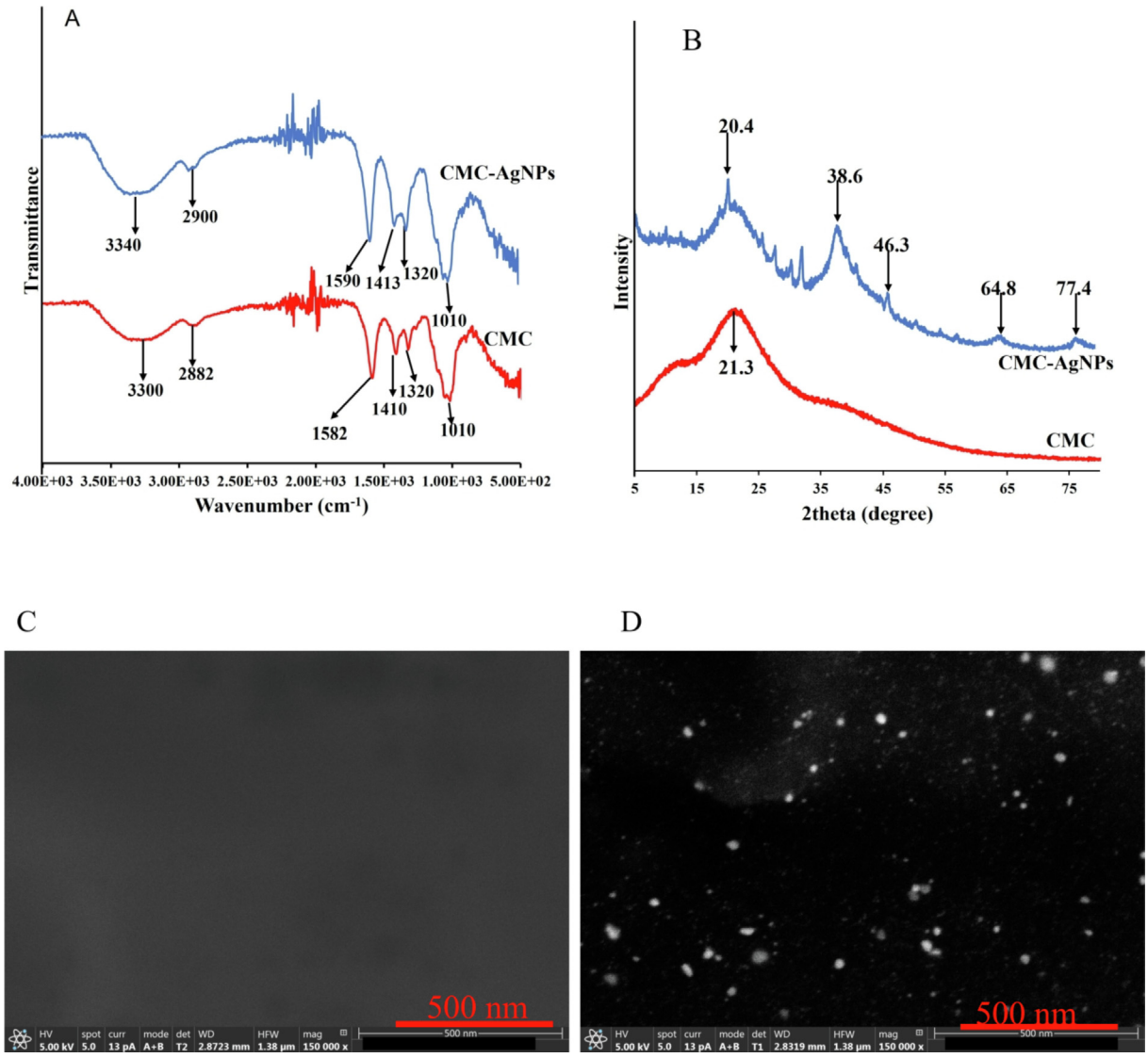


**Fig. 2** (A) ATR-FTIR spectra (B) X-ray diffractogram (XRD) of CMC and CMC-AgNPs. FESEM images of (C) CMC film (D) CMC-AgNPs.

with the generation of $Au^0$. Since the $Hg^{2+}/Hg^0$ standard reduction potential is 0.85 V, also higher than that of Ag, $Hg^{2+}$ can also induce oxidation of CMC-AgNPs, while also forming $Hg^0$ (Sakly et al., 2017). As a result, designing a colorimetric detection of $Au^{3+}$ using only CMC-AgNPS would be difficult to accomplish, owing to the high possibility of $Hg^{2+}$ interference effect. This reality encouraged us to tune CMC-AgNPs based assay, with the use of AA as an external reducing agent. As can be seen, the addition of AA to CMC-AgNPs and NaOH solution imparted absorption spectra increment (Fig. 3(d)), with a slightly more yellowish color, compared to CMC-AgNPs (Fig. 3(d) inset). However, the addition of $Au^{3+}$ to CMC-AgNPs, NaOH, AA aqueous mixture, resulted in the formation of another peak at 540 nm, which is characteristics of localized surface plasmon resonance peak of small sized AuNPs (Fig. 3(e)), with ruby red color (Fig. 3(e) inset). From the foregoing, it can be emphasized that CMC-AgNPs/AA shows fast response to $Au^{3+}$, while forming naked eyes recognizable colors, that can be used to distinguish the analyte detection from other multifarious metal ions.

Since the concentration of AA in the final reaction pot, and the incubation time, will play significant factors in determining the overall sensing response, these parameters were thus optimized.

### *3.3.1. Optimization of detection parameters*

The effect of AA concentrations, in the detection system was optimized, by varying from 0.25 to 10.0 mM, keeping $Au^{3+}$ concentration at 80.0 µM. Fig. 4(A), shows the absorption spectra, where a progressive decrease in the absorption intensity at 403 nm diminishes with an emergence of another peak at 540 nm. The photo images equally showed color changes from yellow to ruby red at 5.0 mM and beyond (Fig. 4(A)inset). The plot of $A_{540}/A_{403}$ against AA concentration is displayed in Fig. 4(B). Accordingly, the ratio increased sharply as AA concentration and peaked at 5.0 mM. This shows there

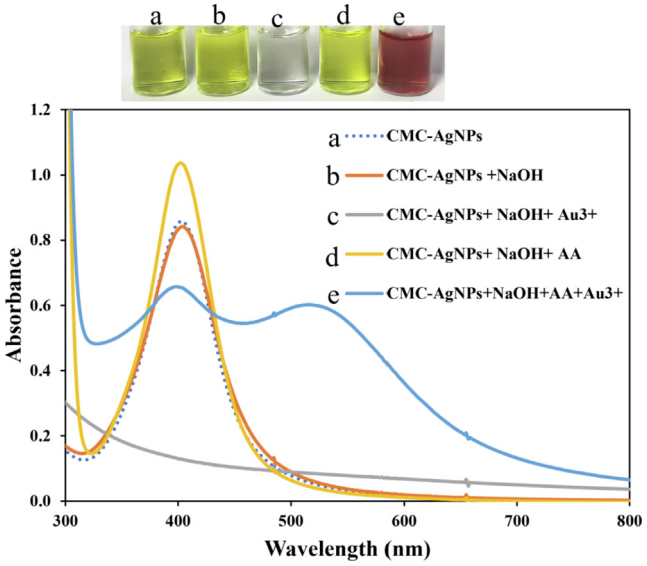


**Fig. 3** Investigation of CMC-AgNPs and AA effects, on colorimetric detection of $Au^{3+}$ (80.0 μM final concentration) in solution.

is an AA concentration saturation at 5.0 mM, and thus was selected for subsequent study.

Appropriate incubation time is important in nanomaterials-based detection to allow for adequate reaction between the analyte and other reacting species. As shown in Fig. S4, the reaction mixture was monitored under three different concentrations of $Au^{3+}$ at 5.0, 40.0 and 100.0 μM, at 2 min interval. As can be seen, the plot of $A_{540}/A_{403}$ against Time, revealed a fast reaction time with saturation at about 8 min, which was thus selected for all studies.

### *3.4. Analytical performance of CMC-AgNPs/AA probe*

#### *3.4.1. Sensitivity*

The sensitivity of CMC-AgNPs/AA nano sensor for $Au^{3+}$ detection was investigated under the optimal detection conditions. In a 2 mL reaction solution, the addition of pH adjusted CMC-AgNPs, AA and $Au^{3+}$, with subsequent vortex mixing and RT incubation for 8 min, a concentration dependent response (naked eye observation) and UV–vis absorption changes were realized. Fig. 4 shows the effect of consistent increment in $Au^{3+}$ concentration from 0.00 to 150.0 μM, on CMC-AgNPs/AA probe. As can be observed, the light-yellow color of CMC-AgNPs/AA, gradually changed to dark yellow, orange, ruby red and purple red color as the concentrations of $Au^{3+}$ increases in the reaction pot (Fig. 5(A)). Fig. 5 (B) shows the absorption spectra of CMC-AgNPs/AA under different concentrations of $Au^{3+}$ ranging from 0.00 to 150.0 μM. As depicted, the absorbance at 403 nm diminished progressively, with the emergence of another at longer wavelength (540 nm), which is attributed to the formation of small sized AuNPs in the reaction pot, deposited on the CMC-AgNPs seed colloidal solution. The plot of $A_{540}/A_{403}$ against $Au^{3+}$ concentrations from 0.00 to 150.0 μM, is revealed in Fig. 5(C), with linear range from 0.25 to 100.0 μM. The absorbance ratios ($A_{540}/A_{403}$) perfectly summed up the analytical response of this assay. The higher the $A_{540}/A_{403}$ ratio, the higher the AuNPs formation in solution and the more deviation from light yellow color. The calibration plot can be fitted into the equation $Y = 0.0108X - 0.006$ or $A_{540}/A_{403} = 0.0108 [Au^{3+}] - 0.006$, with R square value of 0.9937. The limit of detection (LOD) and limit of quantification (LOQ) were calculated using the equations, 3.3xSy/x /slope and 10x Sy/x /slope. Sy/x represent the standard deviation of the regression, and the slope is obtained from the calibration plot (ICH,1996). The LOD and LOQ, was thus estimated as 0.061 and 0.185 μM, respectively.

The analytical features of the CMC-AgNPs/AA probe towards $Au^{3+}$ detection was compared with reported methods and presented in Table 1. As observed, the LOD and linear range of the present detection strategy is comparable or better than previous works (Chen et al., 2018; Gao et al., 2019; Megarajan et al., 2019; Tantubay et al., 2021). While it may be quite challenging applying some of the fluorescence-based assays in water, the present assay is fully operational in an aqueous environment. It is also germane to argue from the perspective of availability and affordability between a visible spec-

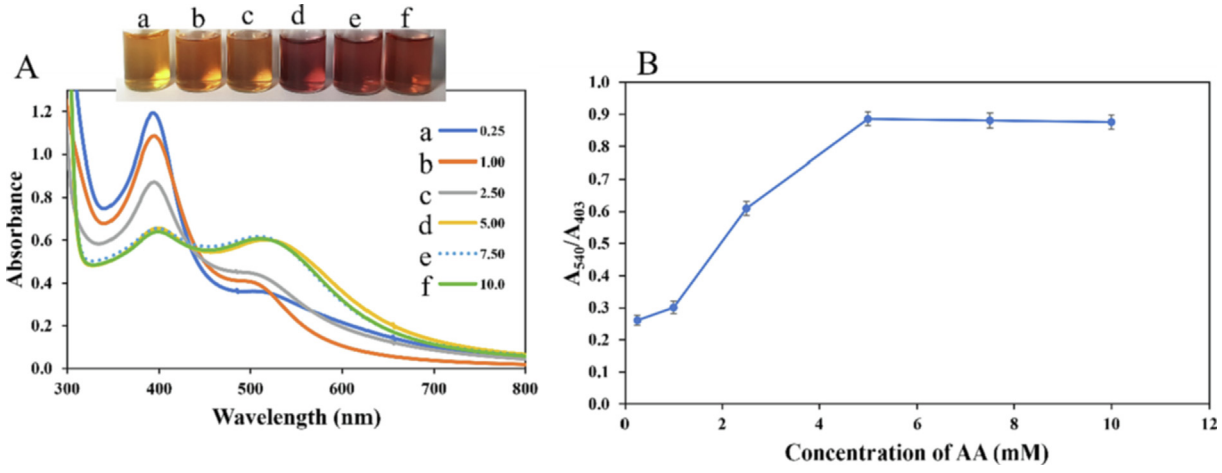


**Fig. 4** (A) UV–vis absorption spectra of CMC-AgNPs probe, under different concentrations of AA, while keeping $Au^{3+}$ concentration at 80.0 μM, inset shows the photo images of a. 0.25b. 1.00c. 2.50 d. 5.00 e. 7.50f. 10.0 mM AA (B) Plot of $A_{540}/A_{403}$ vs AA concentrations.

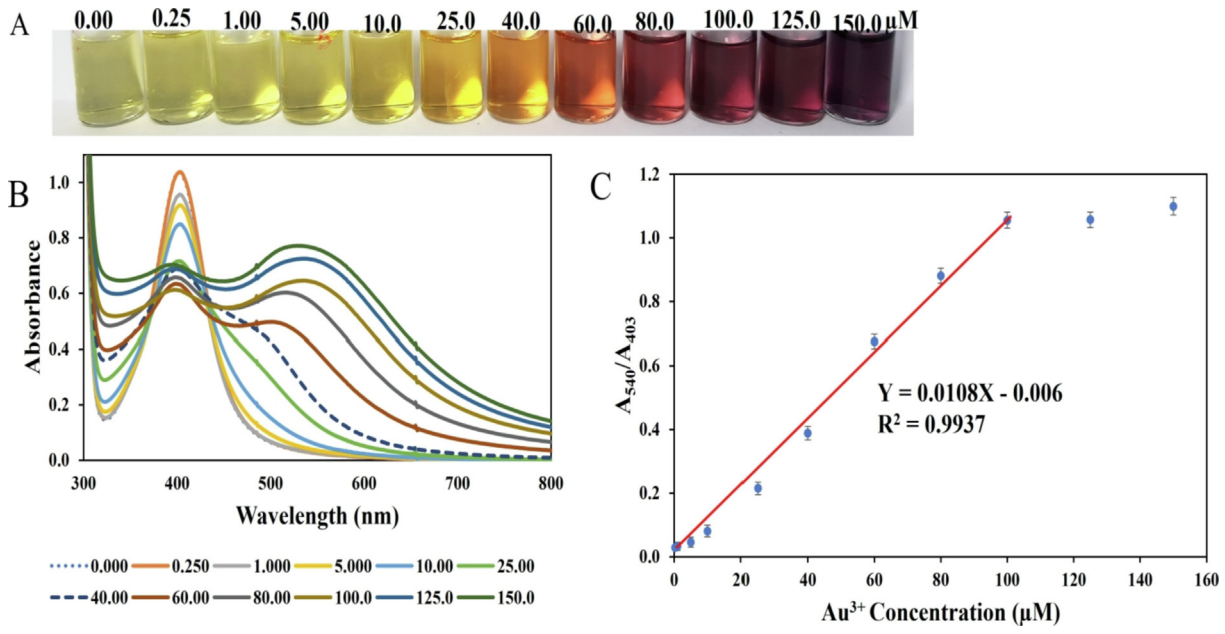


**Fig. 5** (A) Photo images of CMC-AgNPs/AA optical probe, in response to $Au^{3+}$ concentrations from 0.00 to 150.0 µM (B) UV–vis absorption spectra of CMC-AgNPs/AA when charged against $Au^{3+}$ concentration from 0.00 to 150.0 µM (C) Plot of $A_{540}/A_{403}$ against $Au^{3+}$ concentration from 0.00 to 150.0 µM, showing linearity between 0.25 and 100.0 µM.

trophotometer and a fluorimeter. Our method, which is based on UV–visible machine, as read out device, is well more affordable and cost effective than a fluorimeter that is several times more expensive. As a result, this assay can be easily replicated and applied for $Au^{3+}$ monitoring in the environment, especially for economically challenged countries. The naked eye detection capacity of the present assay is far superior to other reported assays. As can be visualized, $Au^{3+}$ concentration as low as 0.25 µM can be obviously distinguished from the blank sample, which further lay credence to the assay's high sensitivity.

We further investigated the possible mechanistic basis of CMC-AgNPs/AA probe for $Au^{3+}$ detection, as follows.

With the use of $NaBH_4$ (a strong chemical reductant), for the synthesis of CMC-AgNPs, rapid reduction of $AgNO_3$ was realized and further validated with the absorption maximum at 403 nm. Thus, the nanoparticles are impregnated in the biopolymer matrix, as shown in Scheme 1. The addition of NaOH solution for pH adjustment, AA-as external reductant, followed by the analyte ($Au^{3+}$), then vortex mixing and allowing RT incubation. A progressive color perturbation was observed, that is dependent on the concentration of $Au^{3+}$ ion added. We propose that the CMC-AgNPs could act as seed material, upon which AA can reduce the added $Au^{3+}$, to form Ag@Au nanostructure, inside CMC matrix i.e. (CMC-Ag@Au nanostructure). The formation of CMC-Ag@Au nanostructure is marked with naked eye observable color changes, that is proportional to the $Au^{3+}$ concentrations. At the low concentration of $Au^{3+}$, small Au shell is formed, consequently, the optical property of the nanomaterial

**Table 1** Comparison of CMC-AgNPs/AA probe with other reported methods for $Au^{3+}$ detection.

| Detection methods/ probe | Limit of detection LOD (µM) | Linear range (µM) | Reference |
|---|---|---|---|
| Electrochemistry [Oligo-adenin nucleotide] | 0.050 | 0.00 – 0.600 | (Wu and Lai, 2016) |
| Fluorimetry [phosphorus-Cdots] | 5.86 | 6.00 – 1000.0 | (Chen et al., 2018) |
| Fluorimetry [GO-PVA] | NA | 0.00 – 300.0 | (Kundu et al., 2012) |
| Fluorimetry | 0.070 | 0.00 – 60.0 | (Kambam et al., 2015) |
| Fluorimetry [N—S Cdots] | 0.063 | 50.0 – 750.0 | (Sharma et al., 2018) |
| Fluorimetry [NeCDs] | 0.016 | 0.00–25 | (Raji et al., 2022) |
| Fluorimetry [HCD & OCD carbon dots] | 3.35 | 0.00 – 80.0 | (Gao et al., 2019) |
| Colorimetry [N10TM-AgNPs] | 3.53 | 3.33–50 | (Megarajan et al., 2019) |
| Colorimetry [Ag/NCNPs] | 0.160 | 0.10 – 2.20 | (Tantubay et al., 2021) |
| Colorimetry [FSN-AuNPs] | 0.050 | 0.10 – 2.50 | (Yang et al., 2013) |
| **Colorimetry [CMC-AgNPs/AA]** | **0.061** | **0.25–100.0** | **This work** |

**FSN-AuNPs** = Fluorosurfactant-capped gold nanoparticles; **Ag/NCNPs** = Silver/Nitrogen-doped Carbon nanoparticles; **N10TM-AgNPs** = *N*-deconyltromethamine functionalized silver nanoparticles; HCD & OCD carbon dots = Hydrophilic and organophilic carbon dots; **NeCDs** = Neem seed derived carbon dots; N—S Cdots = Nitrogen-sulfur co doped carbon dots; **GO-PVA** = Graphene Oxide-Poly(vinyl alcohol) Hybrid; NA = Not available.

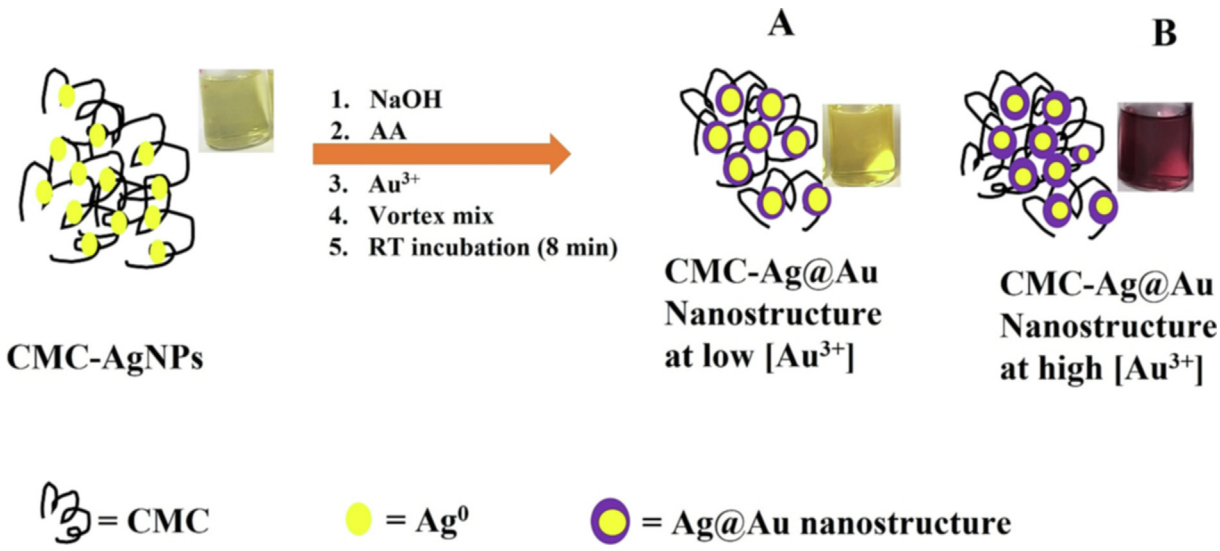


**Scheme 1** Mechanism of CMC-AgNPs/AA based optical nanoprobe for $Au^{3+}$ detection in solution.

is reflective of AgNPs core (yellowish color), Scheme 1, image A. However, at high concentration of the $Au^{3+}$, an immediate yellow color fading of CMC-AgNPs to colorless was observed, then to ruby red or purple red within 8 min. This observation can be explained, based on the formation of high Au shell on CMC-AgNPs core, consequently, Au shell dominate the characteristic color of the formed nanomaterial, hence the strong purple color of AuNPs is observed, Scheme 1, image B.

To buttress the proposed mechanism, we acquired the TEM images, DLS and zeta potential, of CMC-AgNPs under different $Au^{3+}$ treatment, as presented in Fig. 6. The TEM images (Fig. 6(A)) and DLS (Fig. 6(D)) of CMC-AgNPs/AA when treated with no $Au^{3+}$, i.e., blank sample, showed monodispersed morphology, with particle diameter of 80.6 ± 2.5 nm. However, with $Au^{3+}$ injection at 40.0 μM, the TEM image showed spherical particles with decreased morphology (Fig. 6(B)) and an average particle size of 55.5 ± 4.3 nm (Fig. 6(E)). The same trend was observed when $Au^{3+}$ concentration was maintained at 100.0 μM (Fig. 6(C)), while the hydrodynamic size was 45.2 ± 3.5 nm (Fig. 6(F)). The above validated the proposition that at high concentration of $Au^{3+}$, Au shell dominates the optical property of the generated CMC-Ag@Au nanostructure.

The zeta potential of $Au^{3+}$ addition to CMC-AgNPs/AA at 0.00, 40.0 and 100.0 μM is depicted in Fig.S5. Accordingly, the zeta values are quoted at −26.0 ± 2.4, −24.2 ± 1.0 and −23.6 ± 1.1 mV, respectively. This shows the particles are all very stable, though with a decreasing stability from CMC-AgNPs/AA to the $Au^{3+}$ treatment at 100.0 μM.

We further investigated the microstructural property of CMC-AgNPs/AA after $Au^{3+}$ addition at 60.0 μM, by centrifuging the solution and thereafter freeze drying afterwards. The FESEM image as shown in Fig. 6(G) at very high magnification confirmed the formation of spherical nanomaterials, marked with blue arrows, inside the CMC polymer matrix. The EDS spectrum confirmed the presence of elements, such as C, O, Ag and Au (Fig. 6(H)), with higher percentage of Au than Ag (Fig. 6(H)inset). The elemental mapping revealing Ag and Au elements are shown in Fig. 6(I) and (J)), respectively. These observations finally maintained that AA reduced $Au^{3+}$ to AuNPs inside CMC polymer matrix, with concomitant formation of CMC-Ag@Au nanostructure proportionate to $Au^{3+}$ concentration injected in the reaction solution.

### *3.4.2. Precision*

Precision is another important analytical parameter of interest in method development. It is a measure of repeatability and reproducibility of measurements, expressed in relative standard deviation (RSD%). We acquired the UV–vis spectra of $Au^{3+}$ injection at 5.0 and 80.0 μM (high and low concentrations), on CMC-AgNPs/AA for (n = 10) to represent intra-day precision and at three consecutive days as inter-day precision. RSD of 1.3 and 3.6 % were obtained which shows the detection strategy can be easily replicated, at the optimal conditions, without significant variability.

### *3.4.3. Selectivity*

Selectivity of the CMC-AgNPs/AA probe towards $Au^{3+}$ was demonstrated by charging different common metal ions ($Ca^{2+}$, $Mg^{2+}$, $Mn^{2+}$, $Zn^{2+}$, $K^{+}$, $Na^{+}$, $Ba^{2+}$, $Ni^{2+}$, $Ca^{2+}$, $Al^{3+}$, $Cr^{3+}$, $Pb^{2+}$, $Co^{2+}$, $Cd^{2+}$, $Fe^{2+}$, $Fe^{3+}$, $Hg^{2+}$, $Ag^{+}$ and $Au^{3+}$), all at 60.0 μM, similar to previous reports (Bhamore et al., 2021; Shellaiah et al., 2016), then acquiring the photo images and the UV–vis absorption spectra. It is apposite to state here that a 1:1 ratio between the analyte and interfering metal ions, maintained in this work, may be unrealistic in real sample situation, as the interfering may occur at much higher concentrations. As shown in Fig. 7(A), only the presence of $Au^{3+}$ could furnish a ruby red color, in comparison with other metal ions. However, $Ag^{+}$ generated deep yellowish color, while $Hg^{2+}$ induced color change to colorless. This is further revealed in Fig. 7(B), where the UV–vis spectra clearly underscored that only $Au^{3+}$ induced red shift in CMC-AgNPs/AA spectra with a sharp peak at 540 nm. $Ag^{+}$ (Fig. 7(B)blue line), showed peak increment at 403 nm, which may be due to the reduction of $Ag^{+}$ to more AgNPs, that is further deposited on the CMC-AgNPs seed. $Hg^{2+}$ showed a blue shift, thus, the present method is capable of distinguishing between very similar metals ($Au^{3+}$, $Ag^{+}$ and $Hg^{2+}$). The plot

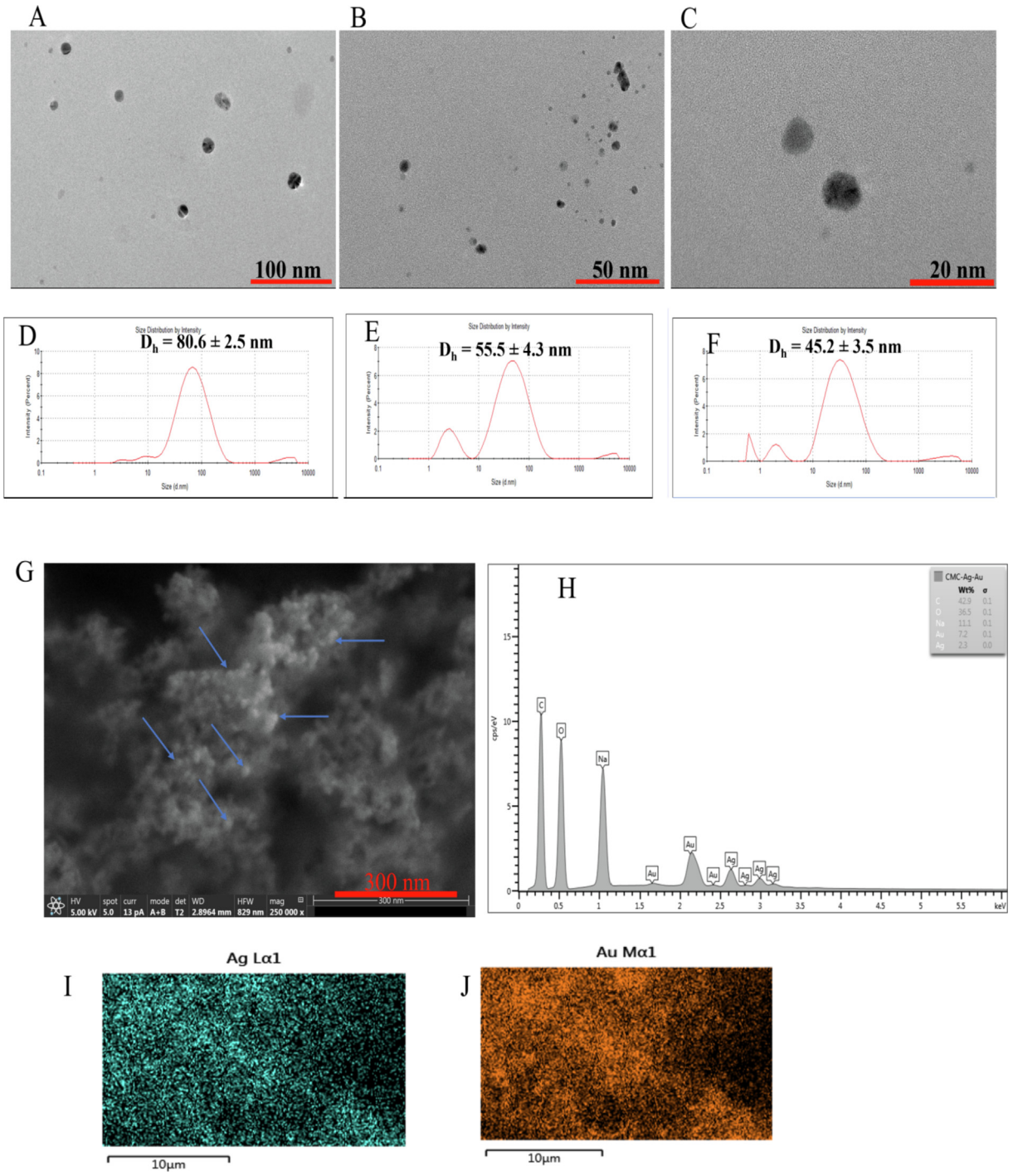


**Fig. 6** TEM images of (A) CMC-AgNPs/AA probe; CMC-AgNPs/AA probe on addition of (B) 40.0 μM (C) 100.0 μM $Au^{3+}$. (D), (E) and (F) are the hydrodynamic diameters from DLS corresponding to the samples (A) (B) and (C) from TEM (G) FESEM image of CMC-AgNPs/AA after $Au^{3+}$ injection at (60.0 μM) (H) EDS Spectrum of CMC-AgNPs/AA after $Au^{3+}$ injection at (60.0 μM), Elemental mapping showing Ag (I) and Au (J).

of $A_{540}/A_{403}$ against all metal ions tested is shown in Fig. 7(C). Only the addition of $Au^{3+}$ could generate a ratio that is significantly different from the blank sample ($p \geq 0.05$). Thus, tuning the CMC-AgNPs/AA probe for $Au^{3+}$ detection by correlating response with AuNPs property is the major strength of this assay. Since AuNPs optical properties is specifically generated from its parent salt ($Au^{3+}$). As a result, this assay showed significant selectivity when compared with other reported detection probes.

### *3.4.4. Real sample application*

To demonstrate the practical application of the probe for $Au^{3+}$ detection, wastewater sample was collected from the Chulalongkorn University campus, Thailand. Demonstration

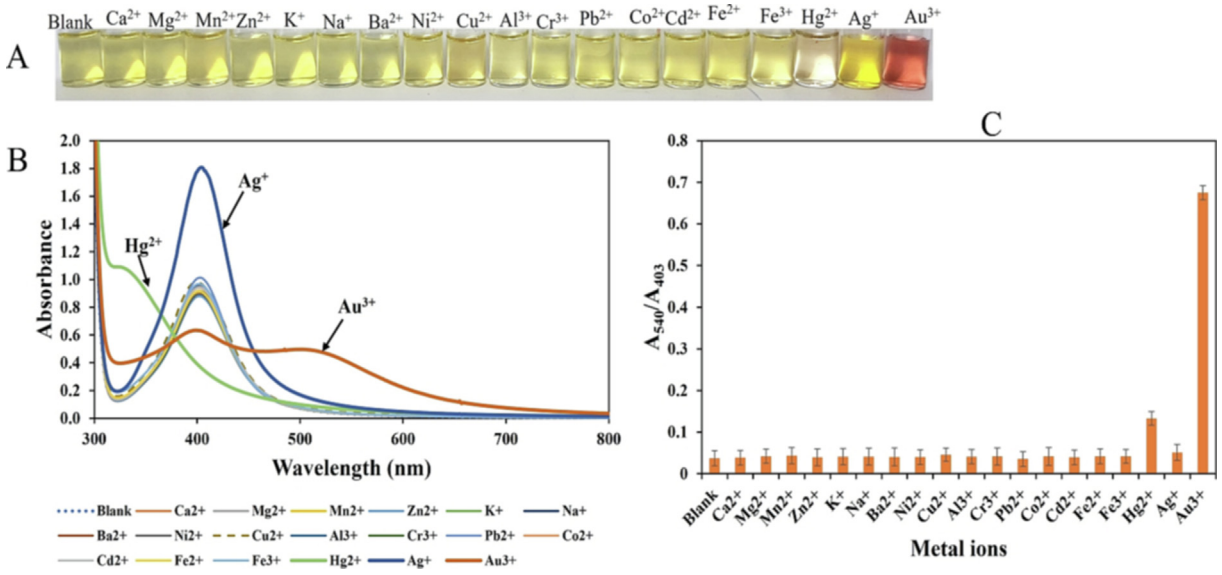


**Fig. 7** (A) Photo images of CMC-AgNPs/AA tested against possible interfering metal ions (Blank, $Ca^{2+}$, $Mg^{2+}$, $Mn^{2+}$, $Zn^{2+}$, $K^{+}$, $Na^{+}$, $Ba^{2+}$, $Ni^{2+}$, $Ca^{2+}$, $Al^{3+}$, $Cr^{3+}$, $Pb^{2+}$, $Co^{2+}$, $Cd^{2+}$, $Fe^{2+}$, $Fe^{3+}$, $Hg^{2+}$, $Ag^{+}$) and $Au^{3+}$ all at 60.0 µM (B) UV–vis absorption spectra of CMC-AgNPs/AA charged against metal ions (C) Plot of $A_{540}/A_{403}$ against tested metal ions at 60.0 µM.

of metal ions in real water samples including, (lake water, drinking water, tap water, river water) is a common approach to investigate detection probe practicality (Li et al., 2022). The water sample was collected in a polypropylene bottle and then refrigerated in the laboratory at 4 °C. Before analysis, the sample was removed from the refrigerator and allowed to maintain RT. It was then centrifuged at 6000 rpm for 20 min to remove all particles, and further passed through a 0.22-µm syringe filter. The processed water was submitted for Au detection using ICP-OES (no Au concentration was detected), while the other part was subjected to $Au^{3+}$ detection using the CMC-AgNPs/AA probe, by adopting the popular standard addition method. Here, different concentrations of $Au^{3+}$ were spiked into the water sample, after which, 50 µL of the prepared samples were charged on the CMC-AgNPs/AA following the steps in section 2.4. The final concentrations of $Au^{3+}$ were maintained within

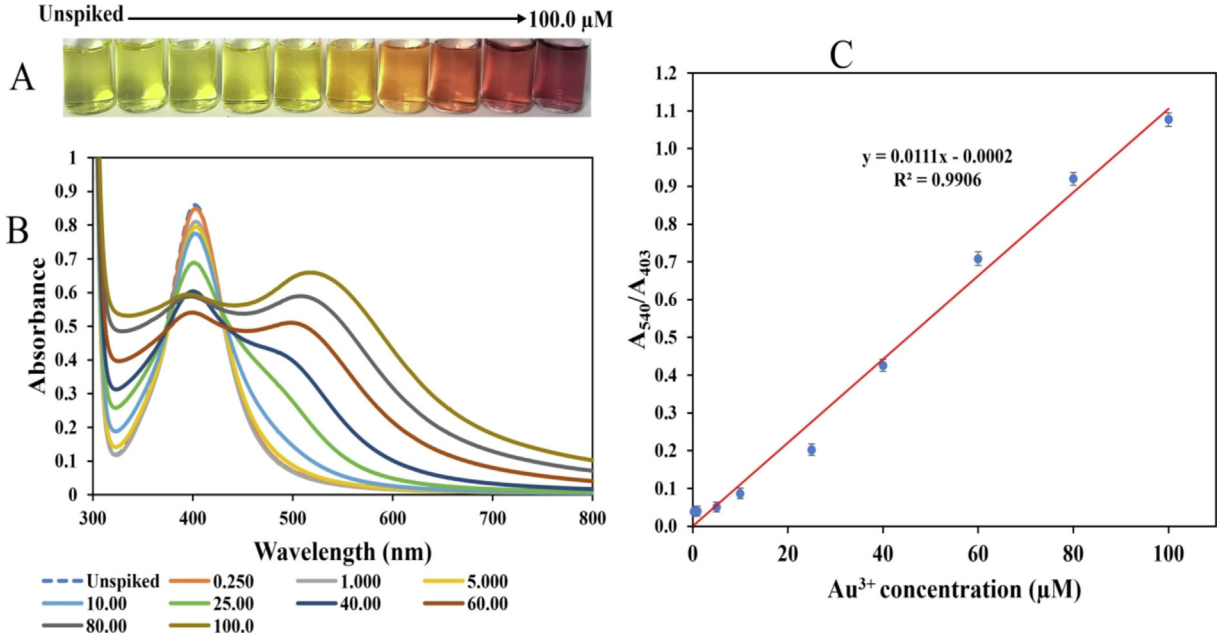


**Fig. 8** (A) photo images (B) UV–vis absorption spectra of CMC-AgNPs/AA probe applied to $Au^{3+}$ detection in wastewater sample, from the unspiked sample to $Au^{3+}$ concentration at 100.0 µM (C) Plot of $A_{540}/A_{403}$ vs $Au^{3+}$ concentrations from 0.25 to 100.0 µM, spiked in wastewater sample.

**Table 2** Determination of $Au^{3+}$ in wastewater sample using CMC-AgNPs/AA probe.

| Concentration added (μM) | Concentration estimated (μM) | Recovery (%) | RSD (%) n = 3 |
|---|---|---|---|
| 0.00 | 0.00 | – | – |
| 5.00 | 4.59 ± 0.12 | 91.8 | 1.8 |
| 40.0 | 38.28 ± 0.09 | 95.7 | 2.7 |
| 100.0 | 103.4 ± 0.14 | 103.4 | 3.6 |

the linear range obtained during the calibration plot (0.25 – 100.0 μM). Fig. 8(A) shows the photo images of $Au^{3+}$ spiked in wastewater sample and the unspiked sample. Accordingly, obvious color changes similar to the progression observed for the calibration plot was realized. This shows the CMC-AgNPs/AA probe can respond to $Au^{3+}$ concentrations ion in complex real sample. The UV–vis absorption spectra were plotted and displayed in Fig. 8(B). The absorbance at 403 nm decreased consistently with an emergence of another peak at 540 nm, while the plot of absorbance ratios $A_{540}/A_{403}$ versus $Au^{3+}$ concentration is shown in Fig. 8(C). The real sample plot furnished an equation, $A_{540}/A_{403} = 0.0111[Au^{3+}] - 0.002$, with $R^2$ value of 0.9906, for $Au^{3+}$ concentrations within 0.25 to 100.0 μM. We further compared the $A_{540}/A_{403}$ for the calibration plot (Std Cal) and the plot in wastewater sample (Real Samp), within the concentration range 0.25 to 100.0 μM, as shown in Fig.S6. Comparison of the responses in the two media using a two-way ANOVA, shows there existed no significant differences ($P \geq 0.05$). Consequently, we estimated the accuracy of the CMC-AgNPs/AA probe towards $Au^{3+}$ detection in wastewater sample using the plot from the real sample plot, by estimating the recovery at $Au^{3+}$ concentrations (0.00, 5.0, 40.0 and 100.0 μM). The percent recovery, calculated using the equation stated in section 2.5, is shown in Table 2, with values ranging between 91.8 and 103.4 %, with RSD less than 4 %, validating the practical effectivity of the probe. This shows the optical probe can effectively respond to $Au^{3+}$ in complex real samples.

## 4. Conclusion

In this work, a sensitive and selective colorimetric strategy was proposed for facile detection of toxic $Au^{3+}$ ion in aqueous environment using CMC-AgNPs. For the realization of CMC-AgNPs with small particles size (less than10 nm), $NaBH_4$ was used for $AgNO_3$ reduction at RT. The synthesized CMC-AgNPs, shows sparkling light-yellow color, with absorption maximum at 403 nm. CMC-AgNPs was further supplemented or supported with AA, an effective biological reducing agent, for the *in-situ* reduction of $Au^{3+}$ (analyte), on the preformed CMC-AgNPs seed. Thus, the addition of $Au^{3+}$ to pH adjusted CMC-AgNPs, with AA addition support in the detection mixture, an efficient colorimetric probe (CMC-AgNPs/AA), was realized. The addition of different concentrations of $Au^{3+}$ to the probe, resulted in RT color perturbation from light yellow, to yellow, orange, red and purple red within 8 min incubation at RT. The absorption spectra red shifted with a new peak development at 540 nm which is characteristic of small sized AuNPs, formed on the CMC-AgNPs. Consequently, CMC-Ag@Au nanostructure was proved to be formed in the detection solution. The detection approach demonstrated high selectivity in comparison with possible interfering metal ions. Linearity between 0.25 and 100.0 μM, and an estimated LOD of 0.061 μM, was realized. The practical usage of the assay was investigated using wastewater sample, through the spiked recovery method, with percent recovery between 91.8 and 103.4 % and RSD less than 4 %. Thus, without complex detection strategy, a sensitive optical probe was proposed for $Au^{3+}$ monitoring in environmental samples with reliable analytical performances.

## CRediT authorship contribution statement

**Titilope John Jayeoye:** Conceptualization, Methodology, Validation, Investigation, Formal analysis, Writing – original draft. **Chamaiporn Supachettapun:** Methodology, Investigation, Writing – review & editing. **Nongnuj Muangsin:** Resources, Writing – review & editing, Supervision.

## Declaration of Competing Interest

The authors declare that they have no known competing financial interests or personal relationships that could have appeared to influence the work reported in this paper.

## Acknowledgement

Dr. Titilope John Jayeoye, would like to appreciate the C2F (The second century fund) Fellowship, Chulalongkorn University, Thailand, for the award of postdoctoral Fellowship and Dr. Fredrick N. Eze of the Drug delivery System Excellence Center, Faculty of Pharmaceutical Sciences, Prince of Songkla University, Hatyai, Thailand, for assistance with samples instrumental characterization.

## Appendix A. Supplementary material

Supplementary data to this article can be found online at https://doi.org/10.1016/j.arabjc.2023.104552.

## References

Afzali, D., Daliri, Z., Taher, M.A., 2014. Flame atomic absorption spectrometry determination of trace amount of gold after separation and preconcentration onto ion-exchange polyethylenimine coated on Al2O3. Arab. J. Chem. 7, 770–774. https://doi.org/10.1016/j.arabjc.2010.12.018.

Asnag, G., Oraby, A.H., Abdelghany, A.M., 2019. Green synthesis of gold nanoparticles and its effect on the optical, thermal and electrical properties of carboxymethyl cellulose. Compos. B: Eng. 172, 436–446. https://doi.org/10.1016/j.compositesb.2019.05.044.

Baghbani-Arani, F., Movagharnia, R., Sharifian, A., Salehi, S., Shandiz, S.A.S., 2017. Photo-catalytic, anti-bacterial, and anti-cancer properties of phyto-mediated synthesis of silver nanoparticles from Artemisia tournefortiana Rchb extract. J. Photochem. Photobiol. B: Biol. 173, 640–649. https://doi.org/10.1016/j.jphotobiol.2017.07.003.

Bhamore, J.R., Gul, A.R., Kailasa, S.K., Kim, K.W., Lee, J.S., Park, H., Park, T.J., 2021. Functionalization of gold nanoparticles using guanidine thiocyanate for sensitive and selective visual detection of Cd2+. Sens. Actuators B: Chem. 334,. https://doi.org/10.1016/j.snb.2021.129685 129685.

Block, W.D., Knapp, E.L.J., 1945. Metabolism, toxicity, and manner of action of gold compounds in the treatment of arthritis: vii. the effect of various gold compounds on the oxygen consumption of rat tissues. J. Pharmacol. Exp. Ther. 83, 275–278.

Chen, Z., Wang, S., Yang, X., 2018. Phosphorus-doped carbon dots for sensing both Au (III) and L-methionine. J. Photochem.

Photobiol. A: Chem. 365, 178–184. https://doi.org/10.1016/j.jphotochem.2018.08.001.

Chen, X., Zhao, X., Wang, G., 2020. Review on marine carbohydrate-based gold nanoparticles represented by alginate and chitosan for biomedical application. Carbohydr. Polym. 244,. https://doi.org/10.1016/j.carbpol.2020.116311 116311.

Corti, C.W., Holliday, R.J., Thompson, D.T., 2002. Developing new industrial applications for gold: gold nanotechnology. Gold Bull. 35, 111–117.

De Góes, R.E., Muller, M., Fabris, J.L., 2017. Spectroscopic detection of glyphosate in water assisted by laser-ablated silver nanoparticles. Sensors 17 (5), 954. https://doi.org/10.3390/s17050954.

de Lima, C.A., da Silva, P.S., Spinelli, A., 2014. Chitosan-stabilized silver nanoparticles for voltammetric detection of nitrocompounds. Sens. Actuators B: Chem. 196, 39–45. https://doi.org/10.1016/j.snb.2014.02.005.

Devi, B.L., Rao, K.M., Ramananda, D., 2020. Spectroscopic investigation of green synthesized ZnS nanoparticles encapsulated by sodium carboxy methyl cellulose. Appl. Phys. A 126, 1–11. https://doi.org/10.1007/s00339-020-04107-y.

Duan, J., Yin, H., Wei, R., Wang, W., 2014. Facile colorimetric detection of Hg2+ based on anti-aggregation of silver nanoparticles. Biosens. Bioelectron. 57, 139–142. https://doi.org/10.1016/j.bios.2014.02.007.

Eze, F.N., Ovatlarnporn, C., Jayeoye, T.J., Nalinbenjapun, S., Sripetthong, S., 2022. One-pot biofabrication and characterization of Tara gum/Riceberry phenolics–silver nanogel: a cytocompatible and green nanoplatform with multifaceted biological applications. Int. J. Biol. Macromol. 206, 521–533. https://doi.org/10.1016/j.ijbiomac.2022.02.140.

Gao, W., Zhou, Y., Xu, C., Guo, M., Qi, Z., Peng, X., Gao, B., 2019. Bright hydrophilic and organophilic fluorescence carbon dots: One-pot fabrication and multi-functional applications at visualized Au3+ detection in cell and white light-emitting devices. Sens. Actuators B: Chem. 281, 905–911. https://doi.org/10.1016/j.snb.2018.11.024.

Hall, G.E., Vaive, J.E.J., 1992. Determination of gold in geological samples by anodic stripping voltammetry at field locations. Chem. Geol. 102, 41–52. https://doi.org/10.1016/0009-2541(92)90145-U.

Hazarika, S.I., Dolai, B., Atta, A.K., 2020. Water compatible triazole linked pyrene-C1-glucosyl fluorescent sensor for Au3+ and living cell imaging studies. J. Mol. Struct. 1202,. https://doi.org/10.1016/j.molstruc.2019.127272 127272.

Huang, P., Liu, B., Jin, W., Wu, F., Wan, Y., 2016. Colorimetric detection of Cd2+ using 1-amino-2-naphthol-4-sulfonic acid functionalized silver nanoparticles. J. Nanopart. Res. 18, 1–9. https://doi.org/10.1007/s11051-016-3630-8.

ICH (1996), International Conference on Harmonisation of Technical Requirements for Registration of Pharmaceuticals for Human Use, Q2B Validation of Analytical Procedures: Methodology. ICH-Q2B, 1–10.

Ismail, M., Khan, M.I., Akhtar, K., Khan, M.A., Asiri, A.M., Khan, S.B., 2018. Biosynthesis of silver nanoparticles: a colorimetric optical sensor for detection of hexavalent chromium and ammonia in aqueous solution. Phys. E: Low-Dimens. Syst. Nanostruct. 103, 367–376. https://doi.org/10.1016/j.physe.2018.06.015.

Jayeoye, T.J., Olatunde, O.O., Benjakul, S., Rujiralai, T., 2020. Synthesis and characterization of novel poly (3-aminophenyl boronic acid-co-vinyl alcohol) nanocomposite polymer stabilized silver nanoparticles with antibacterial and antioxidant applications. Colloids Surf. B: Biointerfaces 193,. https://doi.org/10.1016/j.colsurfb.2020.111112 111112.

Jayeoye, T.J., Eze, F.N., Olatunde, O.O., Benjakul, S., Rujiralai, T., 2021. Synthesis of silver and silver@ zero valent iron nanoparticles using Chromolaena odorata phenolic extract for antibacterial activity and hydrogen peroxide detection. J. Environ. Chem. Eng. 9,. https://doi.org/10.1016/j.jece.2021.105224 105224.

Kambam, S., Wang, B., Wang, F., Wang, Y., Chen, H., Yin, J., Chen, X., 2015. A highly sensitive and selective fluorescein-based fluorescence probe for Au3+ and its application in living cell imaging. Sens. Actuators B: Chem. 209, 1005–1010. https://doi.org/10.1016/j.snb.2014.12.085.

Krajczewski, J., Kołątaj, K., Kudelski, A., 2017. Plasmonic nanoparticles in chemical analysis. RSC Adv. 7 (28), 17559–17576. https://doi.org/10.1039/C7RA01034F.

Kundu, A., Layek, R.K., Kuila, A., Nandi, A.K., 2012. Highly fluorescent graphene oxide-poly (vinyl alcohol) hybrid: an effective material for specific Au3+ ion sensors. ACS Appl. Mater. Interfaces 4, 5576–5582. https://doi.org/10.1021/am301467z.

Li, X., Hu, Q., Yang, K., Zhao, S., Zhu, S., Wang, B., Zhang, Y., Yi, J., Song, X., Lan, M., 2022. Red fluorescent carbon dots for sensitive and selective detection and reduction of Au3+. Sens. Actuators B: Chem. 371,. https://doi.org/10.1016/j.snb.2022.132534 132534.

Lin, L., Peng, S., Shi, C., Li, C., Hua, Z., Cui, H., 2022. Preparation and characterization of cassava starch/sodium carboxymethyl cellulose edible film incorporating apple polyphenols. Int J. Biol Macromol. https://doi.org/10.1016/j.ijbiomac.2022.05.121.

Losev, V. N., Parfenova, V.V., Elsuf'ev, E.V., Borodina, E.V., Metelitsa, S.I., Trofimchuk, A.K., 2020. Separation and preconcentration followed by ICP-OES and ICP-MS determination of precious metals using silica gel chemically modified with dithiocarbamate groups. Sep. Sci Technol. 55, 2659-2669. https://doi.org/10.1080/01496395.2019.1655454.

Madla-Cruz, E., De la Garza-Ramos, M., Romo-Sáenz, C.I., Tamez-Guerra, P., Garza-Navarro, M.A., Urrutia-Baca, V., Martínez-Rodríguez, M.A., Gomez-Flores, R., 2020. Antimicrobial activity and inhibition of biofilm formation in vitro and on human dentine by silver nanoparticles/carboxymethyl-cellulose composites. Arch. Oral Biol. 120,. https://doi.org/10.1016/j.archoralbio.2020.104943 104943.

Megarajan, S., Kamlekar, R.K., Kumar, P.S., Anbazhagan, V., 2019. Rapid and selective colorimetric sensing of Au 3+ ions based on galvanic displacement of silver nanoparticles. New J. Chem. 43, 18741–18746. https://doi.org/10.1039/C9NJ04289J.

Mosaviniya, Kikhavani, T., Tanzifi, M., Yaraki, M.T., Tajbakhsh, P., Lajevardi, A., 2019. Facile green synthesis of silver nanoparticles using Crocus Haussknechtii Bois bulb extract: Catalytic activity and antibacterial properties. Colloid Interface Sci Commun. 33, 100211. https://doi.org/10.1016/j.colcom.2019.100211.

Paramelle, D., Sadovoy, A., Gorelik, S., Free, P., Hobley, J., Fernig, D.G., 2014. A rapid method to estimate the concentration of citrate capped silver nanoparticles from UV-visible light spectra. Analyst 139, 4855–4861. https://doi.org/10.1039/C4AN00978A.

Prema, P., Veeramanikandan, V., Rameshkumar, K., Gatasheh, M.K., Hatamleh, A.A., Balasubramani, R., Balaji, P., 2022. Statistical optimization of silver nanoparticle synthesis by green tea extract and its efficacy on colorimetric detection of mercury from industrial waste water. Environ. Res. 204,. https://doi.org/10.1016/j.envres.2021.111915 111915.

Qin, S., Yu, X., Xu, L., 2021. Amplified fluorescence detection and adsorption of Au3+ by the fluorescent melamine formaldehyde microspheres incorporated with N and S co-doped carbon dots. J. Hazard. Mater. 405,. https://doi.org/10.1016/j.jhazmat.2020.123978 123978.

Rajar, K., Alveroglu, E., Caglar, M., Caglar, Y., 2021. Highly selective colorimetric onsite sensor for Co2+ ion detection by povidone capped silver nanoparticles. Mater. Chem. Phys. 273,. https://doi.org/10.1016/j.matchemphys.2021.125082 125082.

Raji, K., Thiyagarajan, S.K., Suresh, R., Vadivel, R., Palanivel, D., Ramamurthy, P., 2022. Neem seed derived green C-dots: a highly sensitive luminescent probe for aqueous Au3+ ions and nurtures green gold recovery. Colloids Surf. A: Physicochem. Eng. Asp. 641,. https://doi.org/10.1016/j.colsurfa.2022.128523 128523.

Sakly, N., Marzouk, W., Ouada, H.B., Majdoub, H., 2017. Enhancing performances of colorimetric response of carboxymethylcellulose-stabilized silver nanoparticles: a fully eco-friendly assay for Hg2+ detection. Sens. Actuators B: Chem. 253, 918–927. https://doi.org/10.1016/j.snb.2017.07.035.

Santos, K. d. O., Elias, W.C., Signori, A.M., Giacomelli, F.C., Yang, H., Domingos, J.B., 2012. Synthesis and catalytic properties of silver nanoparticle–linear polyethylene imine colloidal systems. J. Phys Chem C 116, 4594-4604. https://doi.org/10.1021/jp2087169.

Sharma, V., Kaur, N., Tiwari, P., Saini, A.K., Mobin, S.M., 2018. Multifunctional fluorescent "Off-On-Off" nanosensor for Au3+ and S2− employing NS co-doped carbon–dots. Carbon 139, 393–403. https://doi.org/10.1016/j.carbon.2018.07.004.

Shellaiah, M., Simon, T., Sun, K.W., Ko, F.H., 2016. Simple bare gold nanoparticles for rapid colorimetric detection of Cr3+ ions in aqueous medium with real sample applications. Sens. Actuators B: Chem. 226, 44–51. https://doi.org/10.1016/j.snb.2015.11.123.

Tantubay, S., Kalita, H., Pathak, A., 2021. Sensitive detection of auric and sulphide ions using hybrid silver/nitrogen-doped carbon nanoparticles. Sens. Actuators B: Chem. 330,. https://doi.org/10.1016/j.snb.2020.129276 129276.

Wang, L.Y., Wang, M.J., 2016. Removal of heavy metal ions by poly (vinyl alcohol) and carboxymethyl cellulose composite hydrogels prepared by a freeze–thaw method. ACS Sustain. Chem. Eng. 4 (5), 2830–2837. https://doi.org/10.1021/acssuschemeng.6b00336.

Wu, Y., Lai, R.Y.J., 2016. Electrochemical gold (III) sensor with high sensitivity and tunable dynamic range. Anal. Chem. 88, 2227–2233. https://doi.org/10.1021/acs.analchem.5b03868.

Xu, J., Zhang, B., Jia, L., Bi, N., Zhao, T., 2020. Metal-enhanced fluorescence detection and degradation of tetracycline by silver nanoparticle-encapsulated halloysite nano-lumen. J. Hazard. Mater. 386, 121630.

Yang, K., Pan, L., Gong, L., Liu, Q., Li, Z., Wu, L., He, Y., 2018. Colorimetric and visual determination of Au (III) ions using PEGylated gold nanoparticles. Microchim. Acta 185, 1–8. https://doi.org/10.1007/s00604-017-2648-7.

Yang, B., Zhang, X.B., Liu, W.N., Hu, R., Tan, W., Shen, G.L., Yu, R.Q., 2013. Fluorosurfactant-capped gold nanoparticles-based label-free colorimetric assay for Au3+ with tunable dynamic range via a redox strategy. Biosens. Bioelectron. 48, 1–5. https://doi.org/10.1016/j.bios.2013.03.044.

Zeng, Y., Hu, R., Wang, L., Gu, D., He, J., Wu, S.Y., Ho, H.P., Li, X., Qu, J., Gao, B.Z., Shao, Y., 2017. Recent advances in surface plasmon resonance imaging: detection speed, sensitivity, and portability. Nanophotonics 6, 1017–1030. https://doi.org/10.1515/nanoph-2017-0022.

Zhou, X., Xu, W., Liu, G., Panda, D., Chen, P., 2010. Size-dependent catalytic activity and dynamics of gold nanoparticles at the single-molecule level. J. Am. Chem. Soc. 132 (1), 138–146. https://doi.org/10.1021/ja904307n.